Computers and Fluids Vol. 8, pp. 213–223
Pergamon Press Ltd., 1980. Printed in Great Britain

NUMERICAL SOLUTION OF RECIRCULATING FLOW BY A SIMPLE FINITE ELEMENT RECURSION RELATION

D. W. PEPPER and R. E. COOPER
Savannah River Laboratory, E. I. du Pont de Nemours and Company, Aiken, SC 29801, U.S.A.

(*Received* 2 *July* 1979)

Abstract—A time-split finite element recursion relation, based on linear basis functions, is used to solve the two-dimensional equations of motion. Recirculating flow in a rectangular cavity and free convective flow in an enclosed container are analyzed. The relation has the advantage of finite element accuracy and finite difference speed and simplicity. Incorporating dissipation parameters in the functionals decreases numerical dispersion and improves phase lag.

INTRODUCTION

Although finite element recursion relations are not new, their use in simulating fluid flows has been limited. Time-split finite element recursion relations have the advantage of finite element accuracy and finite difference simplicity. The time-splitting feature of the recursion relations allows two-or three-dimensional equations to be solved with a basic one-dimensional algorithm. The resulting systems of equations are tridiagonal, which are easily and efficiently formulated and solved.

A simple recursion relation based on linear interpolation functionals (chapeau functions) with extensions to higher order functionals was formulated for the one-dimensional advection-diffusion equation[1]. The methodology has been applied to geophysical problems and multi-dimensional transport[2–9]. Similar procedures with cubic spline interpolation functionals have been analyzed by Rubin and Khosla[10]; compact schemes are discussed by Adam[11].

Recirculating flow problems have been studied both experimentally and numerically for some time. Two particular types of recirculating flow problems that have received considerable attention are cavity flow and free convection flow in enclosed containers. Experimental, analytical, and numerical results are well known for a wide range of conditions. Both problems lend themselves to testing and verifying new and improved numerical schemes. These two problems are used to test the accuracy and applicability of the time-split finite element recursion algorithm to describe fluid motion.

PROBLEM

The laminar motion of an incompressible, constant property, Newtonian fluid in a square cavity and in an enclosed rectangular box is analyzed. The flow in the square cavity is induced by the top wall moving in its own plane; the flow in the enclosed box is induced by thermal gradients between the hot and cold walls. Figure 1 shows the physical geometry of both problems.

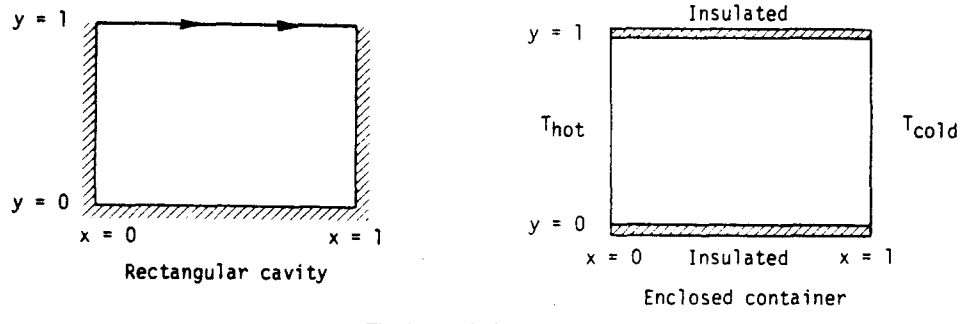

Fig. 1. Physical geometries.

The governing equations can be expressed as follows:

For cavity flow

$$\nabla^2\Psi = -\omega \tag{1}$$

$$\frac{\partial\omega}{\partial t} + \frac{\partial u\omega}{\partial x} + \frac{\partial v\omega}{\partial y} = \frac{1}{Re}\nabla^2\omega \tag{2}$$

$$u = \frac{\partial\Psi}{\partial y} \text{ and } v = -\frac{\partial\Psi}{\partial x} \tag{3}$$

where Ψ, u, v and ω are dimensionless streamfunction, horizontal and vertical velocity components, and vorticity, respectively; Re denotes the Reynolds number. The boundary conditions to be satisfied are $u(0,y) = u(1,y) = v(x,0) = v(x,1) = 0$; and $u(x,1) = 1$.

For enclosed free convective flow

$$\frac{\partial\omega}{\partial t} + \frac{\partial u\omega}{\partial x} + \frac{\partial v\omega}{\partial y} = Pr\nabla^2\omega + PrRa\frac{\partial T}{\partial x} \tag{4}$$

$$\frac{\partial T}{\partial t} + \frac{\partial uT}{\partial x} + \frac{\partial vT}{\partial y} = \nabla^2 T \tag{5}$$

where T is the dimensionless temperature, Pr is the Prandtl number, and Ra is the Rayleigh number. Equation (1) is also used in the equation set. Boundary conditions are $u(0,y) = u(1,y) = v(x,0) = v(x,1) = 0$; $T(0,y) = 1$ and $T(1,y) = 0$; and $\partial T/\partial y(x,0) = \partial T/\partial y(x,1) = 0$. Equation (1) is solved by the cyclic reduction technique[12, 13]. Equations (2), (4) and (5) are solved by the method of fractional steps and the finite element recursion relation. Equation (1) can also be solved by the method of fractional steps with a false transient term.

The recursion relation is based on the linear basis functional algorithm for the one-dimensional advection–diffusion equation[14]. By using hypermatrix methodology[15] coupled with the Galerkin-weighted residual technique, a tridiagonal recursion relation can be obtained that is valid for variable element length and nonuniform velocity. For equal element length and constant velocity, the relation is fourth order accurate in space. A detailed derivation of the relation, including accuracy analysis, is given in[14]. The relation has been applied to the three-dimensional transport of atmospheric pollutants[9].

The basic recursion relation is written for one-dimensional transport[14] as follows

$$\begin{aligned}&\frac{1}{6}[\dot\phi_{i-1}\Delta x_- + 2\dot\phi_i(\Delta x_+ + \Delta x_-) + \dot\phi_{i+1}\Delta x_+]\\ &\quad + \frac{1}{6}[\phi_{i-1}(-u_{i-1} - 2u_i) + \phi_i(u_{i-1} - u_{i+1}) + \phi_{i+1}(2u_i + u_{i+1})]\\ &\quad + k\left[-\frac{\phi_{i-1}}{\Delta x_-} + \phi_i\left(\frac{1}{\Delta x_+} + \frac{1}{\Delta x_-}\right) - \frac{\phi_{i+1}}{\Delta x_+}\right] = 0\end{aligned} \tag{6}$$

where u_i is the velocity at node point i, ϕ is either vorticity or temperature; $\dot\phi$ denotes a time derivative; $i-1$, i and $i+1$ are node point locations; and k is either $1/Re$, Pr or 1 according to the specific equation being solved. For one-dimensional uniform element length, eqn (6) becomes

$$\begin{aligned}&\frac{1}{6}[\dot\phi_{i-1} + 4\dot\phi_i + \dot\phi_{i+1}] + \frac{1}{6\Delta x}[\phi_{i-1}(-u_{i-1} - 2u_i) + \phi_i(u_{i-1} - u_{i+1})\\ &\quad + \phi_{i+1}(2u_i + u_{i+1})] + \frac{k}{\Delta x^2}[-\phi_{i-1} + 2\phi_i - \phi_{i+1}] = 0.\end{aligned} \tag{7}$$

To reduce numerical dispersion errors associated with solution of eqn (7), the initial value and advection terms are modified to

$$\left[\left(\frac{\Delta x}{6}+\frac{\rho}{2}\right)\dot{\phi}_{i-1}+\frac{2\Delta x}{3}\dot{\phi}_i+\left(\frac{\Delta x}{6}-\frac{\rho}{2}\right)\dot{\phi}_{i+1}\right]$$
$$+\frac{2}{\Delta x}\left\{\phi_{i-1}\left[-u_{i-1}-2u_i-\frac{\rho}{2}\left(\frac{u_i+u_{i-1}}{\Delta x}\right)\right]+\phi_i\left[u_{i-1}-u_{i+1}\right.\right.$$
$$\left.+\frac{\rho}{2}\left(\frac{u_{i+1}+2u_i+u_{i-1}}{\Delta x}\right)\right]+\phi_{i+1}\left[2u_i+u_{i+1}\right.$$
$$\left.\left.-\frac{\rho}{2}\left(\frac{u_i+u_{i+1}}{\Delta x}\right)\right]\right\}+\frac{k}{\Delta x^2}(-\phi_{i-1}+2\phi_i-\phi_{i+1})=0 \tag{8}$$

where ρ is a dissipation function with $\rho=\rho(\Delta x)$. This particular filtering scheme was used by Raymond and Garder[3] to eliminate troublesome dispersive waves in telescoping meshes. ρ acts as an artificial diffusion coefficient of $0(\Delta x^3)$ and effectively damps short waves while minimally affecting the desired longer wave distribution[3, 9]. By optimally selecting the best value for ρ, phase lag can be improved without significant computational damping. Test results are given in the Appendix.

Since eqn (7) involves $i-1$, i, and $i+1$ nodal points, eqn (7) can be written in the general form (modified by eqn (8)).

$$A\phi_{i-1}+B\phi_i+C\phi_{i+1}-D=0 \tag{9}$$

where the coefficients A, B, C and D are defined as

$$A=1+\frac{3\rho}{\Delta x}+\frac{\Delta t}{2\Delta x}\left[-2u_i-u_{i-1}-\frac{3\rho}{\Delta x}(u_i+u_{i-1})\right]-\frac{3\Delta t}{Re\Delta x^2}$$

$$B=4+\frac{\Delta t}{2\Delta x}\left[(u_{i-1}-u_{i+1})+\frac{3\rho}{\Delta x}(u_{i+1}+2u_i+u_{i-1})\right]+\frac{6\Delta t}{Re\Delta x^2}$$

$$C=1-\frac{3\rho}{\Delta x}+\frac{\Delta t}{2\Delta x}\left[2u_i+u_{i+1}-\frac{3\rho}{\Delta x}(u_i+u_{i+1})\right]-\frac{3\Delta t}{Re\Delta x^2}$$

$$D=\left\{-4+\frac{\Delta t}{2\Delta x}\left[(u_{i-1}-u_{i+1})+\frac{3\rho}{\Delta x}(u_{i+1}+2u_i+u_{i-1})\right]\right.$$
$$\left.+\frac{6\Delta t}{Re\Delta x^2}\right\}\omega_i^n+\omega_{i-1}^n\left\{-1-\frac{3\rho}{\Delta x}+\frac{\Delta t}{2\Delta x}\left[-2u_i-u_{i-1}\right.\right.$$
$$\left.\left.-\frac{3\rho}{\Delta x}(u_i+u_{i-1})\right]-\frac{3\Delta t}{Re\Delta x^2}\right\}+\omega_{i+1}^n\left\{-1+\frac{3\rho}{\Delta x}\right.$$
$$\left.+\frac{\Delta t}{2\Delta x}\left[2u_i+u_{i+1}-\frac{3\rho}{\Delta x}(u_i+u_{i+1})\right]-\frac{3\Delta t}{Re\Delta x^2}\right\} \tag{10}$$

where ω^n denotes vorticity values obtained at the previous time step (with Crank–Nicolson time averaging), and Δt is the time step increment. A similar expression is written for the vertical component. Equations (4) and (5) can be solved either with the Thomas algorithm or with bi- or tri-tridiagonal solution algorithms[16, 17]. The algorithm can be extended readily to three-dimensional flow by the time-split procedure[14]. Investigations are being undertaken to simulate free convective flow in three dimensions.

RESULTS

Cavity flow

The equation set for laminar recirculating flow in a square cavity was solved for Reynolds numbers of 100, 400, 1000 and 2000. Numerous numerical simulations exist in the literature for $100 \leq Re \leq 1000$; Nallasamy and Prasad[18] present results for $Re > 1000$.

In three test cases, a grid (element) spacing of 1/20 was used with $\rho = 0.001$, and a 21×21 mesh. The optimum time step, Δt, was chosen for each test case to minimize the number of iterations required for convergence. Figure 2 shows contours of streamfunction and velocity vectors. At $Re = 100$, two small recirculation zones are generated in the lower left and right hand corners with a large primary cell generated in the center. Steady-state solutions were obtained in 154 time steps (approximately 18 sec CPU for IBM 360/195) with a Δt of 0.15. When the Re is increased to 400, the right lower corner cell begins to enlarge, displacing the lower streamlines of the large primary cell upward (and causing the vortex center to move). Steady-state conditions were obtained after 205 time steps (~ 23 sec CPU) with a Δt of 0.20. At $Re = 1000$, the lower right corner cell has enlarged along with a noticeable increase in the size of the lower left corner cell. The solution converged in 849 time steps (~ 86 sec) with a Δt of

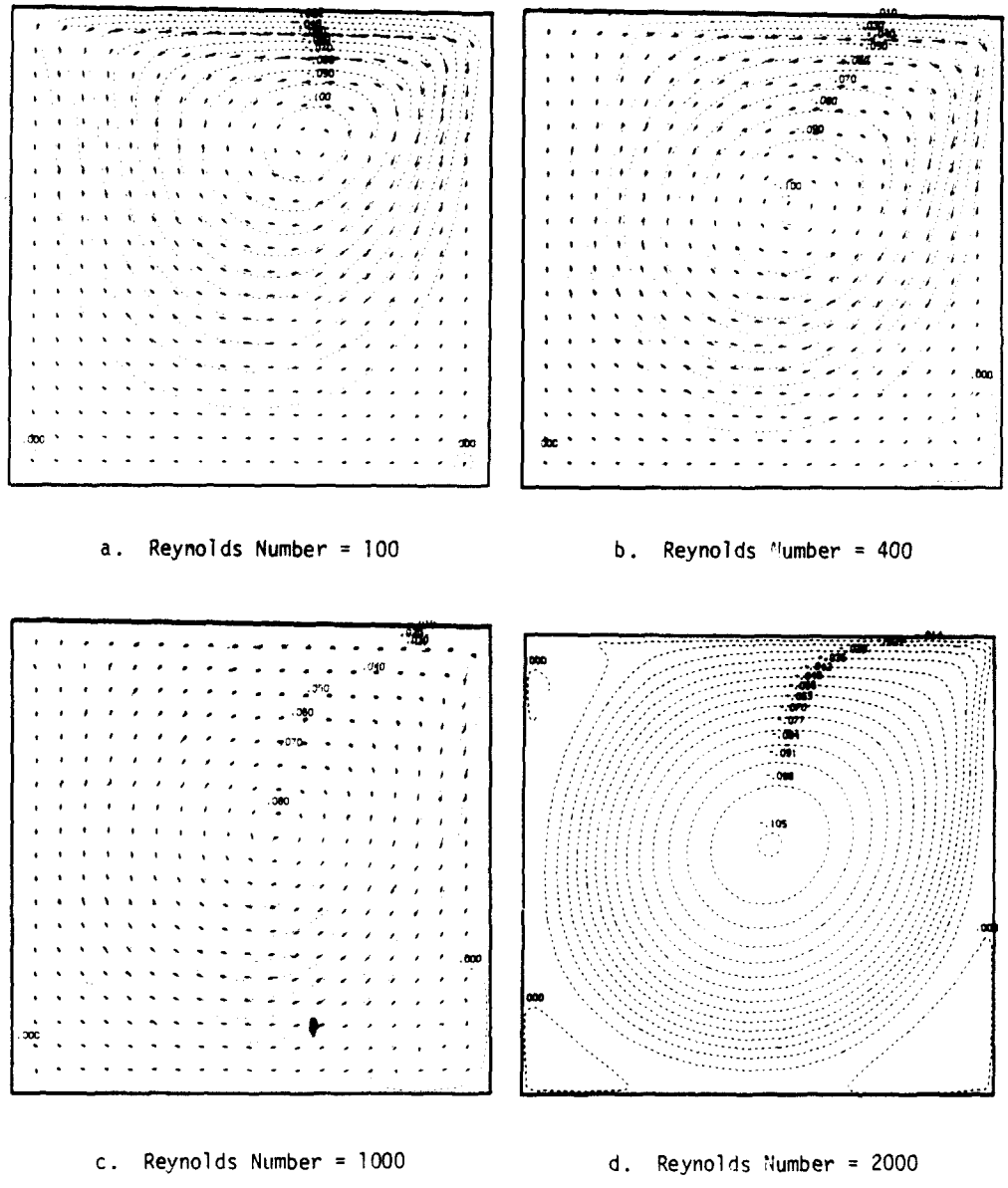

Fig. 2. Driven cavity flow—streamfunction isopleths and velocity vectors.

0.10. Stream-function and vorticity values at the primary vortex centers for $100 \leq Re \leq 1000$ are in good agreement with results obtained by others[18–21]. Specific values are compared in Table 1.

Results obtained at $Re = 2000$ were questionable with the 21×21 mesh. The cellular pattern of the flow was synonymous with the onset of small-scale numerical disturbances (which lead to instability). Attempts to obtain convergence with heavier dissipation control, $\rho \geq 1$, were not successful. This lack of convergence for the smaller mesh was due to the influence of the wall boundary layer development on the recirculation pattern as $Re > 1000$. Further refinement of the grid spacing (51×51) helped to more accurately resolve the steep gradients near the boundaries. Tests with variable grid spacing would also resolve the gradients near the wall, but truncation error drops from fourth order to first order for the spatial derivative terms.

Results in Ref.[18] were obtained by upwind differencing methods, which are known to exhibit stability control at the expense of computational damping errors [22]. Such errors can lead to large secondary cells which are physically unrealistic.

Free convective flow

Steady-state solutions to the governing equation set for laminar natural convection in a square cavity were obtained for three separate test cases—each solution beginning with zero initial conditions for ψ and ω. Figure 3 shows streamfunction-velocity vector plots and isotherms for Rayleigh number simulations of 10^3, 10^4 and 10^5, respectively. Computation times were under two minutes for a 21×21 mesh. One large single cell is produced in the first two simulations, the cell strength increasing as the Rayleigh number is increased. At $Ra = 10^5$, two distinct cells are generated shortly after the calculation is begun which persists until convergence is achieved; this is in agreement with previously published solutions for $Ra = 10^5$ and indicates the development of multicellular flow at moderate Ra values. Further tests are being conducted with higher order functionals in an effort to obtain numerical solutions for Ra values greater than 10^6 (without some form of upwind/damping scheme).

A plot of the average Nusselt number vs Rayleigh number is shown in Fig. 4. The average Nusselt number was obtained from

$$Nu = \int_0^1 \left.\frac{\partial T}{\partial x}\right|_{x=0} \mathrm{d}x \tag{11}$$

with the integral calculated by Simpson's rule at both the left and right vertical walls and the values averaged. Results obtained by eqn (11) are in good agreement with previously published values.

Table 1. Square cavity flow comparisons

Re	Reference	Grid	Primary Vortex ψ	Primary Vortex ω
100	[19]	8	0.1035	3.098
	[21]	51	0.1032	--
	[20]	41	0.1015	3.143
	[18]	51	0.1026	3.155
	Present	21	0.1086	2.957
400	[19]	8	0.1168	2.415
	[18]	51	0.1014	2.114
	[20]	41	0.1017	2.142
	[24]	21	0.1030	2.170
	Present	21	0.1064	2.070
1000	[19]	8	0.1299	2.653
	[18]	51	0.0977	1.830
	[21]	51	0.0812	--
	Present	21	0.0803	1.550
2000	[18]	51	0.0951	1.570
	Present	51	0.1053	1.800

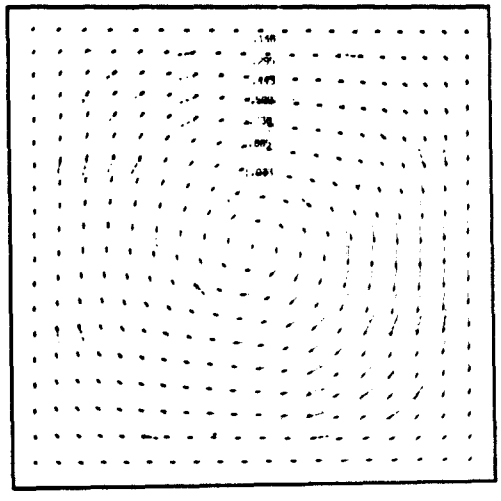

a. Rayleigh Number = 1000

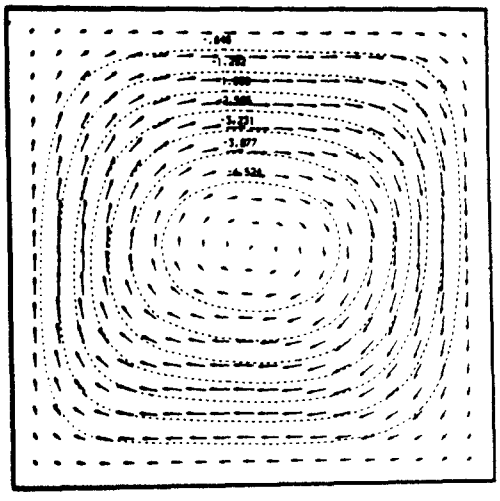

b. Rayleigh Number = 10,000

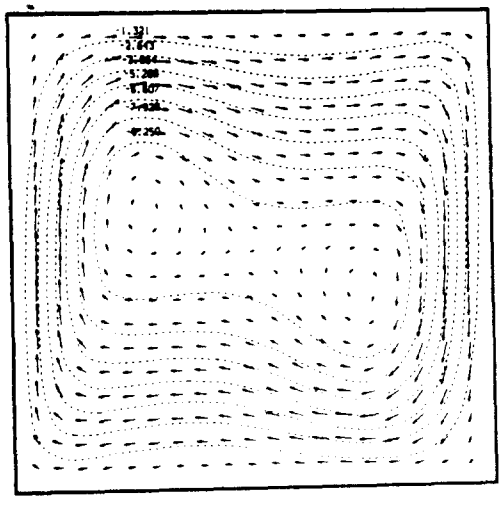

c. Rayleigh Number = 100,000

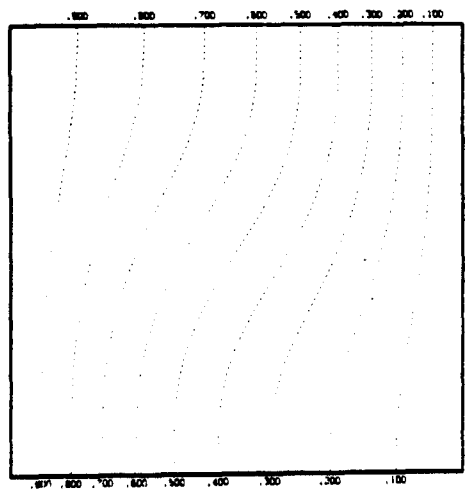

d. Rayleigh Number = 1000

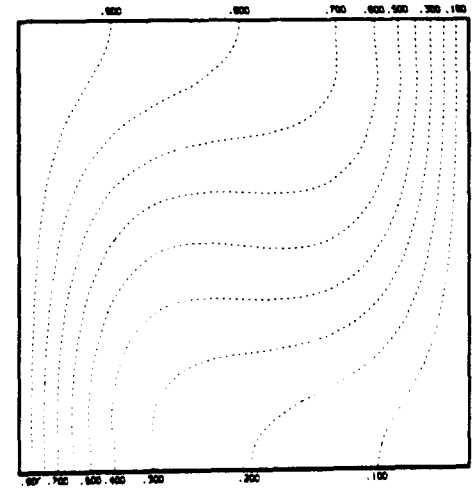

e. Rayleigh Number = 10,000

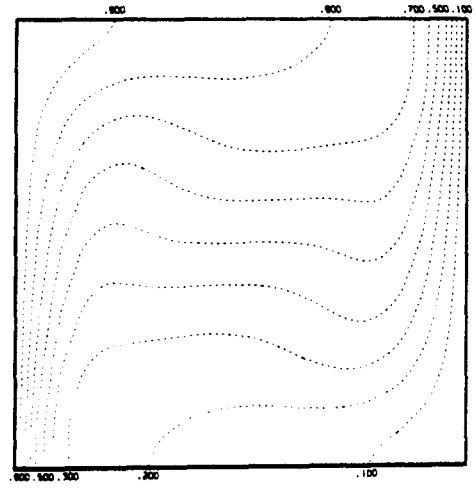

f. Rayleigh Number = 100,000

Fig. 3. Free convection flow—streamfunction isopleths, velocity vectors and temperature isopleths.

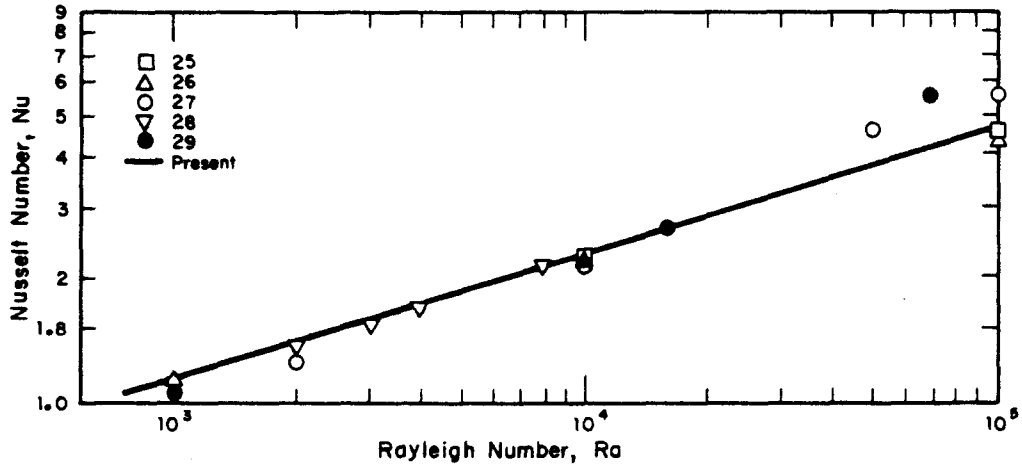

Fig. 4. Average Nusselt number.

CONCLUSION

A simple finite element recursion relation has been used to calculate recirculating flows in rectangular cavities and enclosed containers with differential heating. The numerical algorithm is based on one-dimensional linear element basis functions. The algorithm is extended to two dimensions by the technique of fractional steps (time-splitting). Numerical dispersion errors are controlled by incorporating dissipation terms within the basis functionals. These terms selectively damp (filter) shortwave noise without significantly damping the longer wavelengths; an improvement in phase lag also results.

Results for two-dimensional flow in a cavity and free convective flow in an enclosure are in agreement with results available in the literature. Speed, accuracy, and simplicity of the algorithm make its use in three-dimensional calculations appealing. Preliminary simulations of three-dimensional free convective flows are promising.

Table 2. Free convection flow comparisons

Ra	Reference	Grid	Primary Vortex ψ
10^3	[25]	64 (9-node element)	1.18
	[27]	11	1.17
	Present	21	1.18
10^4	[25]	64	5.12
	[27]	11	6.249
	Present	21	5.17
10^5	[25]	64	9.54
	[27]	11	7.786
	Present	21	10.57

Acknowledgement—The information contained in this article was developed during the course of work under Contract No. AT(07-2)-1 with the U.S. Department of Energy.

REFERENCES

1. H. S. Price, J. C. Cavendish and R. S. Varga, Numerical methods of higher order accuracy for diffusion-convection equations. *Soc. Pet. Engng J.* **243**, 293–303 (1968).
2. P. E. Long and F. J. Hicks, *Simple Properties of Chapeau Functions and Their Application to the Solution of the Advection Equation.* National Oceanic and Atmospheric Administration TDL Office Note 75-8, Silver Spring, Maryland 23 pp. (1975).
3. W. H. Raymond and A. Garder, Selective damping in a Galerkin method for solving wave problems with variable grids, *Mon. Weather Rev.* **104**, 1583–1590 (1976).
4. P. E. Long, Jr. and D. W. Pepper, A comparison of six numerical advection schemes for calculating the advection of atmospheric pollution. *Proc. 3rd Symp. Atmos. Turbulence, Diffusion and Air Quality*, Rayleigh, North Carolina, America. Meterology Society, 181–187 (1976).
5. M. J. P. Cullen, On the use of artificial smoothing in Galerkin and finite differencing solutions of the primitive equation, *Quart. J. Royal Meteor. Soc.* **102**, 77–93 (1976).
6. R. L. Lee, P. M. Gresho and R. L. Sani, A comparative study of certain finite element and finite difference methods in advection-diffusion simulation. *USERDA Rep.* UCRL-77539 (1976).
7. P. M. Gresho, R. L. Lee amd R. L. Sani, Modeling the planetary boundary layer using the Galerkin finite-element method. *USERDA Rep.* UCRL-78120 (1976).
8. P. E. Long, Jr. and W. A. Schaffer, Some physical and numerical aspects of boundary layer modeling. *NOAA Tech. Memorandum* NWS TDL-56, Silver Spring, Maryland 27 pp (1975).
9. D. W. Pepper, C. D. Kern and P. E. Long, Jr., Modeling the dispersion of atmospheric pollution using cubic splines and chapeau functions. *Atmos. Environ.* **13**, 223–237 (1979).
10. S. G. Rubin and P. K. Khosla, Higher-order numerical solutions using cubic splines. *AIAA J.* **14**, 851 (1976).
11. Y. Adam, Highly accurate compact implicit methods and boundary conditions. *J. Comp. Phys.* **24**, 10–22 (1977).
12. D. W. Pepper and S. D. Harris, Numerical simulation of natural convection in closed containers by a fully implicit method. *J. Fluids Engng* **99**, 649–656 (1977).
13. P. Swarztrauber and R. Sweet, Efficient FORTRAN subprograms for the solution of elliptic partial differential equations. *NCAR Technical Note*, NCAR-TN/1A-109 (1975).
14. D. W. Pepper and A. J. Baker, A simple one-dimensional finite element algorithm with multi-dimensional capabilities. *Num. Heat Transfer*, **1**, 1–10 (1979).
15. A. J. Baker and M. O. Soliman, Accuracy, convergence and utility of finite element generated solution algorithms for initial-value problems (submitted to *J. Comp. Phys.*).
16. S. G. Rubin and R. A. Graves, Jr., Viscous flow solution with a cubic spline approximation. *Computers and Fluids* **3**, 1–36 (1975).
17. D. V. Von Rosenberg. *Methods for the Numerical Solution of Partial Differential Equations.* Elsevier, New York (1969).

18. M. Nallasamy and K. Krishna Prasad, On cavity flow at high Reynolds numbers. *J. Fluid Mech.* **79**(2), 391–414 (1977).
19. Shih-Yu Tuann and M. D. Olson, Review of computing methods for recirculating flows. *J. Comp. Phys.* **29**, 1–9 (1978).
20. O. R. Burggraf, Analytical and numerical studies of the structure of steady separated flows. *J. Fluid Mech.* **24**(1), 113–151 (1966).
21. J. D. Bozeman and C. Dalton, Numerical study of viscous flow in a cavity. *J. Comp. Phys.* **12**, 348 (1973).
22. P. J. Roache, *Computational Fluid Dynamics*. Hermosa, Albuquerque, New Mexico (1972).
23. J. E. Dendy, Two methods of Galerkin type achieving optimum L^2 rates of convergence for first order hyperbolics. *Siam J. Num. Analy.* **11** (1974).
24. D. W. Pepper and R. E. Cooper, Numerical solutions for a general set of problems by an alternating strongly implicit procedure. Presented at the *Int. Conf. on Num. Methods in Laminar and Turbulent Flow*. Swansea, England, 18–21 July (1978).
25. R. S. Marshall, J. C. Heinrich and O. C. Zienkiewicz, Natural convection in a square enclosure by a finite-element, penalty function method using primitive fluid variables. *Num. Heat Transfer* **1**, 315–330 (1978).
26. B. Roux, J. C. Grondin, P. Bontoux and B. Gilly, On a high-order accurate method for the numerical study of natural convection in a vertical cavity. *Num. Heat Transfer* **1**, 331–349 (1978).
27. G. De Vahl Davis, Laminar natural convection in an enclosed rectangular cavity. *Int. J. Heat Mass Transfer* **11**, 1675–1692 (1968).
28. J. O. Wilkes and S. W. Churchill, The finite difference computation of natural convection in a rectangular enclosure. *AIChE J.* **12**, 161–166 (1966).
29. J. Ozoe, H. Sayama and S. W. Churchill, Natural convection in an inclined square channel. *Int. J. Heat Mass Transfer* **17**, 401–406 (1974).

APPENDIX

The Galerkin procedure requires the residual in the chapeau approximation to be orthogonal to all the basis functions, i.e. i.e.

$$\int \mathrm{d}x R(x, t) e_j(x) = 0 \tag{A1}$$

where $R(x, t)$ is the residual and $e_j(x)$ is the basis function. The imbedding of the dissipation parameter, ρ, is based on the technique derived in [3, 23] such that

$$\int \mathrm{d}x R(x, t)\left[e_j(x) + \rho \frac{\mathrm{d}e_j(x)}{\mathrm{d}x}\right] = 0. \tag{A2}$$

Integration of the one-dimensional advection–diffusion equation is thus altered to

$$\int \left(\frac{\partial \phi}{\partial t} + u\frac{\partial \phi}{\partial x} - k\frac{\partial^2 \phi}{\partial x^2}\right)\left(e_i + \rho \frac{\mathrm{d}e_i}{\mathrm{d}x}\right) \mathrm{d}x = 0. \tag{A3}$$

We first let

$$\begin{aligned} \phi^*(x, t) &= \lfloor e_j(x) \rfloor \{\phi(t)\} \\ \frac{\partial \phi^*(x, t)}{\partial t} &= \lfloor e_j(x) \rfloor \{\phi(t)\}' \\ \frac{\partial \phi^*(x, t)}{\partial x} &= \frac{\mathrm{d}}{\mathrm{d}x} \lfloor e_j(x) \rfloor \{\phi(t)\} \\ u^*(x) &= \lfloor e_j(x) \rfloor \{u\} \end{aligned} \tag{A4}$$

where $e_j(x) = a(t) + b(t)x$ is a linear basis.function, $\{\ \}$ denotes a column matrix, and $\lfloor\ \rfloor$ denotes a row matrix. Applying the Galerkin weighted residual method and making use of integration by parts yield the equation (omitting subscript j and (x))

$$\begin{aligned} &\int \{e\}\lfloor e \rfloor \, \mathrm{d}x \{\phi\}' + \int \rho \{e\}' \lfloor e \rfloor \, \mathrm{d}x \{\phi\}' + \int \{e\}\lfloor e \rfloor \{u\} \lfloor e \rfloor' \, \mathrm{d}x \{\phi\} \\ &\quad + \int \rho \{e\}' \lfloor e \rfloor \{u\} \lfloor e \rfloor' \, \mathrm{d}x \{\phi\} + k \int \{e\}' \lfloor e \rfloor' \, \mathrm{d}x \{\phi\} = 0 \end{aligned} \tag{A5}$$

where e' denotes $\mathrm{d}e/\mathrm{d}x$; boundary value terms have been neglected. The diffusion term of eqn (A5) does not include a dissipation component since it would involve a second derivative of the basis function; this derivative vanishes for a linear basis function. The integrals are easily determined with the use of natural coordinates and hypermatrix methodology, [14, 15]. Assemblage of the technique over two adjacent elements (involving $i-1$, i, and $i+1$ node points) yields eqn (8). As shown in eqn (A5) introduction of the dissipation parameter produces alterations in the initial value and advection terms; it is these terms which are the most troublesome.

The dissipation parameter not only selectively damps the short wave components, but also improves phase lag errors. These two characteristics can be demonstrated by analyzing the one-dimensional advection equation

$$\frac{\partial \phi}{\partial t} + U\frac{\partial \phi}{\partial x} = 0. \tag{A6}$$

By performing a Taylor series expansion on eqn (A6), after employing eqns (A4) and (A5) to determine the recursion form (eqn (8)), eqn (A6) becomes

$$\frac{\partial \phi}{\partial t} + U\frac{\partial \phi}{\partial x} = -k\frac{\partial^4 \phi}{\partial x^4} \tag{A7}$$

where $k = rU\Delta x^3/12$ and $r = \rho/\Delta x$. A solution to eqn (A7) is

$$\phi(x, t) = e^{i\lambda(x-Ut)}e^{-\lambda^4 kt} \tag{A8}$$

where λ is the wave number ($\lambda = 2\pi/L$, L = wavelength), $i = \sqrt{(-1)}$, and t is time. Waves tend to travel at the phase speed U but with the short wavelength selectively damped by the λ^4 term.

Amplification factors are obtained for three numerical techniques used to solve eqn (A6): 1. a forward-in-time, centered-in-space Crank–Nicolson solution (FTCS-CN); 2. a chapeau function solution based on eqn (A7) with $\rho = 0$; 3. a chapeau function solution based on eqn (A7) with $\rho > 0$[3, 23]. The amplification factors are given for each method as

$$\text{1. FTCS-CN} \quad g = \frac{1 - \frac{Ri}{2}\sin\lambda}{1 + \frac{Ri}{2}\sin\lambda} \tag{A9}$$

$$\text{2. Chapeau} \quad g = \frac{4 + 2\cos\lambda - 3i\sin\lambda}{4 + 2\cos\lambda + 3i\sin\lambda} \tag{A10}$$

$$\text{3. Dendy} \quad g = \frac{4 + 2\cos\lambda - 3i(R + 2\rho)\sin\lambda - 12\rho R\sin^2\frac{\lambda}{2}}{4 + 2\cos\lambda + 3i(R - 2\rho)\sin\lambda + 12\rho R\sin^2\frac{\lambda}{2}} \tag{A11}$$

where R is the Courant number ($R = (U\Delta t/\Delta x)$), λ is the wave number and ρ is the dissipation function. Once the amplification factors are obtained, the phase lag can be calculated from

$$C = \frac{\tan^{-1}(g_{imag}/g_{real})}{\lambda\Delta t}. \tag{A12}$$

Comparisons of phase lag vs wave number are given in Table A1 for the three methods for a Courant number of 0.50. The optimum value for $\rho(0.33)$ was determined by trial and error and is a function of the Courant number. Ideally all the waves should travel at a phase speed of $C/U = 1.0$. In the chapeau and FTCS-CN methods, the shortest waves clearly lag the longer waves. Improvement in the phase lag is quite evident in the modified chapeau method (Dendy), particularly for the shortest waves (2.25–4.00 Δx).

The effect of varying ρ on the convergence to steady state conditions for flow in a cavity was also investigated. Table A2 shows the number of time steps required to achieve convergence for a residual of 10^{-4} with ρ varied from 0 to 0.1. Best results were obtained with $\rho \simeq 0.001$. The effects of varying ρ on the maximum streamfunction values were approximately 4%.

Table A1. Phase lag ($R = 0.50$)

Wavelength (Δx)	*FTCS-CN*	*Chapeau ($\rho = 0$)*	*Dendy ρ=0.33 (optimum)*
2.00	0.000	0.0	0.000
2.25	0.122	0.34	0.976
2.50	0.232	0.564	0.972
2.75	0.326	0.698	0.968
3.00	0.407	0.780	0.966
3.50	0.532	0.869	0.967
4.00	0.623	0.913	0.969
5.00	0.743	0.953	0.976
6.00	0.814	0.970	0.981
8.00	0.891	0.985	0.992
10.00	0.928	0.991	0.997
20.00	0.981	0.997	0.999
40.00	0.995	0.999	0.999
80.00	0.998	0.999	0.999

Table A2. Convergence of solutions for $\epsilon = 10^{-4}$ and optimum Δt

Re	Δt	ρ	Iterations	Max ψ
100	0.15	0	154	0.1086
		0.0001	155	0.1086
		0.001	154	0.1086
		0.01	154	0.1088
		0.1	150	0.1102
400	0.20	0	208	0.1064
		0.0001	207	0.1064
		0.001	205	0.1064
		0.01	206	0.1068
		0.1	227	0.1092
1000	0.10	0	842	0.803
		0.0001	892	0.803
		0.001	849	0.803
		0.01	863	0.806
		0.1	794	0.833